Inorganic Chemistry

Article

pubs.acs.org/IC

$[Ni(HF_2)(3\text{-}Clpy)_4]BF_4$ (py = pyridine): Evidence for Spin Exchange Along Strongly Distorted F···H···F$^-$ Bridges in a One-Dimensional Polymeric Chain

Jamie L. Manson,*[,†] Adora G. Baldwin,[†] Brian L. Scott,[‡] Jesper Bendix,[§] Rico E. Del Sesto,[‡] Paul A. Goddard,[∥] Yoshimitsu Kohama,[⊥] Hope E. Tran,[†] Saman Ghannadzadeh,[∥] John Singleton,[⊥] Tom Lancaster,[∥,▽] Johannes S. Möller,[∥] Stephen J. Blundell,[∥] Francis L. Pratt,[⊗] Vivien S. Zapf,[⊥] Jinhee Kang,[△] Changhoon Lee,[△] Myung-Hwan Whangbo,[△] and Christopher Baines[#]

[†]Department of Chemistry and Biochemistry, Eastern Washington University, Cheney, Washington 99004, United States

[‡]Materials Physics and Applications and [⊥]National High Magnetic Field Laboratory, Los Alamos National Laboratory, Los Alamos, New Mexico 87545, United States

[§]Department of Chemistry, University of Copenhagen, Copenhagen DK-2100, Denmark

[∥]Clarendon Laboratory, Department of Physics, University of Oxford, OX1 3PU, U.K.

[⊗]ISIS Pulsed Muon Facility, Rutherford-Appleton Laboratory, Chilton, Oxfordshire, OX11 0QX, U.K.

[△]Department of Chemistry, North Carolina State University, Raleigh, North Carolina 27695, United States

[#]Swiss Muon Source, Paul Scherrer Institut, CH-5253, PSI Villigen, Switzerland

Supporting Information

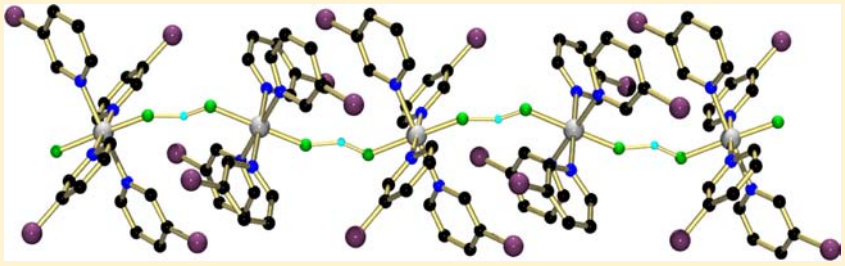

ABSTRACT: $[Ni(HF_2)(3\text{-}Clpy)_4]BF_4$ (py = pyridine) is a simple one-dimensional (1D) coordination polymer composed of compressed NiN_4F_2 octahedra that form chains with bridging HF_2^- ligands. In spite of significant distortion of the HF_2^- bridge, a quasi-1D antiferromagnetic (AFM) behavior was observed with J_{FHF} = 4.86 K.

INTRODUCTION

For several decades, the chemical bond character of the bifluoride molecule (HF_2^- or FHF^-) has been debated.[1] However, most theoretical studies consider HF_2^- to possess the strongest known hydrogen bonds with values ranging between 169 to 241 kJ/mol. From gas-phase ion-cyclotron resonance experiments, a bond enthalpy of 163 kJ/mol was found.[2]

Our research interests lie in the combined use of coordinate covalent and strong hydrogen bonds (F···H···F and F···H−O) so as to fabricate novel magnetic solids.[3−7] To this end, we have synthesized and characterized several coordination polymers, including $Cu(HF_2)_2(pyz)$[3] and the family $[Cu(HF_2)(pyz)_2]X$ (pyz = pyrazine; $X = BF_4^-$, PF_6^-, SbF_6^-, and TaF_6^-),[4] the latter of which possess three-dimensional (3D) frameworks composed of two-dimensional (2D) $[Cu(pyz)_2]^{2+}$ square lattices that are bridged by HF_2^- ligands.

In the $[Cu(HF_2)(pyz)_2]X$ system, the HF_2^- ligand coordinates to the Cu(II) ion along the elongated axial direction (which coincides with the spin-paired d_{z^2} orbital), thus rendering it problematic to assess the efficiency of Cu-FHF-Cu interactions. Because of this, we sought to explore other transition metals that contain multiple magnetic orbitals.

The octahedral Ni(II) ion (S = 1) was particularly appealing as both the $d_{x^2-y^2}$ and d_{z^2} orbitals contain an unpaired electron. Indeed, this was found to be the case in the 3D antiferromagnetic (AFM) $[Ni(HF_2)(pyz)_2]ZF_6$ (Z = P, Sb) metal−organic frameworks. For the PF_6 system, two polymorphic forms (α and β) have been identified; the α-phase containing bent Ni−F−H bonds whereas the β-phase consists of linear Ni−F−H bonds.[5,6] Despite the relatively high T_N's of 6.2 K (α-PF_6), 7.0 K (β-PF_6), and 12.2 K (SbF_6), predominant one-dimensional (1D) magnetism occurs with the Ni-FHF-Ni spin exchange being much stronger (J_{FHF} = 6.1, 7.7, and 11.3 K for α-PF_6, β-PF_6, and SbF_6, respectively) than Ni-pyz-Ni (calculated $J_{pyz} \sim 2$ K).[5,6] In addition, the Ni(II) ion

Received: January 16, 2012
Published: June 29, 2012

   dx.doi.org/10.1021/ic300111k | *Inorg. Chem.* 2012, 51, 7520−7528

experienced single-ion anisotropy leading to zero-field splitting (ZFS), with $D < 0$ (α-PF_6) and $D > 0$ (β-PF_6 and SbF_6).

To better examine the spin exchange along Ni-FHF-Ni pathways, we sought to reduce the lattice and spin dimensionality of $[Ni(HF_2)(pyz)_2]X$ by chemical substitution of the bridging pyz ligands for monodentate 3-chloropyridine (3-Clpy). The sterically hindered 3-Clpy ligand was selected with the aim to provide large interchain spacings. We synthesized $[Ni(HF_2)(3\text{-Clpy})_4]BF_4$ from a reaction mixture that contained $Ni(BF_4)_2$, NH_4HF_2, and 3-Clpy.

Indeed, X-ray structural studies on $[Ni(HF_2)(3\text{-Clpy})_4]BF_4$ reveal the desired 1D chain motif. We recognize that 1D quantum AFM chains containing $S = 1$ spins are known to exhibit a Haldane gap in their excitation spectrum and a magnetically disordered ground state,[8,9] in contrast to half-integer spin chains which show gapless excitations. However, the gapped state in $S = 1$ chains will not be achieved if there exists single-ion anisotropy and/or interchain interactions of sufficient strength, as evidenced by mean-field[10] and quantum Monte Carlo calculations.[11] The absence of a gap in our magnetization data {compare, for example $[Ni(C_2H_8N_2)_2(NO_2)]ClO_4$ (NENP)}[12] and the D/J_{FHF} ratio found in $[Ni(HF_2)(3\text{-Clpy})_4]BF_4$ (see below) leads us to conclude that this system does not exhibit a Haldane state, but the weakness of interchain couplings prevent condensation of a magnetically ordered phase in the temperature range studied.

EXPERIMENTAL SECTION

Synthesis. $Ni(BF_4)_2{\cdot}6H_2O$ (0.4001 g, 1.18 mmol) and NH_4HF_2 (0.0673 g, 1.18 mmol) were dissolved together in a minimal amount of distilled water. To this was added 5 mL of neat 3-chloropyridine to afford a medium blue solution. The solution was covered with a perforated sheet of Parafilm and allowed to slowly evaporate at room temperature. Upon standing for ~2 weeks, X-ray quality blue crystals were recovered from the reaction mixture in high yield (>75%). The crystals were somewhat sensitive to solvent loss, but their integrity could be maintained by storage in a small amount of the mother liquor. Selected IR data (neat, cm^{-1}): 3543 (w), 3319 (w, br), 3074 (w), 2739 (w, br), 1592 (m), 1569 (m), 1464 (s), 1415 (s), 1198 (w), 1118 (s), 1060 (vs), 1031 (vs), 1014 (vs), 815 (vs), 804 (vs), 697 (vs), 637 (vs).

Optical Spectroscopy. Mid-IR spectra were recorded on a Thermo Avatar 360 FT-IR equipped with a Nicolet Smart DuraSamplIR ATR accessory. The sample consisted of a neat powder pressed against a single-bounce diamond crystal. UV−vis−NIR spectra were collected on a Harrick Praying Mantis diffuse-reflectance apparatus mounted in a Varian Cary 5000 UV−vis spectrometer. Baseline corrected reflectance was measured for the sample. The baseline involved 0 and 100% absorbance values for a reference using an empty sample holder and KBr powder, respectively. Spectra were obtained in reflectance mode and converted to absorbance using a standard algorithm.

X-ray Crystallography. A suitable crystal was mounted in a nylon cryoloop. Data were collected using a Bruker D8 diffractometer furnished with an APEX II CCD detector and Bruker Kryoflex low-temperature device. The instrument was equipped with a graphite monochromated Mo$K\alpha$ X-ray source (λ = 0.71073 Å) and a 0.5 mm monocapillary. A hemisphere of data was collected using ω-scans, with 10-s frame exposures and 0.5° frame widths. Data collection, initial indexing, and cell refinement were handled using APEX II software.[13] Frame integration, including Lorentz-polarization corrections, and final cell parameter calculations were carried out using the SAINT+ software.[14] The data were corrected for absorption using redundant reflections and the program SADABS.[15] Decay of reflection intensity was not observed as monitored via analysis of redundant frames. The structure was solved using direct methods and difference Fourier techniques. The bifluoride proton was located on the difference map and refined with a fixed isotropic temperature factor. The remaining hydrogen atoms were placed in idealized positions and allowed to ride on the atom to which they were attached. Final refinement included anisotropic thermal factors for all non-hydrogen atoms. Structure solution, refinement, graphics, and creation of publication materials were performed using the SHELXTL suite.[16] Details of the crystallographic refinement and a list of selected bond lengths and angles are given in Tables 1 and 2, respectively.

Table 1. X-ray Crystallographic Data for $[Ni(HF_2)(3\text{-Clpy})_4]BF_4$

T (K)	140(1)
empirical formula	$C_{20}H_{17}BCl_4F_6N_4Ni$
formula weight (g/mol)	638.68
space group	$P2_1/c$
a (Å)	16.411(6)
b (Å)	12.449(5)
c (Å)	12.291(5)
β (deg)	100.003(4)
V (Å^3)	2473.0(16)
Z	4
D_c (g/cm^3)	1.715
λ (Å)	0.71073
μ (mm^{-1})	1.280
crystal size (mm^3)	0.22 × 0.20 × 0.12
$F(000)$	1280
T_{max}, T_{min}	0.8615, 0.7659
θ_{min}, θ_{max} (deg)	2.06, 28.23
no. total refls.	27011
no. unique refls., R_{int}	5822, 0.0425
no. obsd refls. [$I \geq 2\sigma(I)$]	4628
R_1, wR_2 [$I \geq 2\sigma(I)$]^a	0.0393, 0.0957
R_1, wR_2 (all data)^b	0.0553, 0.1011
GOF	1.322
$\Delta\rho$ (e/Å^3)^c	1.166, −0.831

$^a R = \sum||F_o| - |F_c||/\sum|F_o|$. $^b wR = [\sum w[|F_o| - |F_c|]^2/\sum w[|F_o|^2]]^{1/2}$. ^{c}Max. and min residual electron density.

Table 2. Selected Bond Lengths (Å) and Bond Angles (deg) for $[Ni(HF_2)(3\text{-Clpy})_4]BF_4$

Ni−F1	1.967(2)	N1−C1	1.344(3)
Ni−F2	2.096(2)	N1−C5	1.344(3)
Ni−N1	2.127(2)	C1−C2	1.373(3)
Ni−N2	2.134(2)	C2−Cl1	1.726(3)
Ni−N3	2.110(2)	C2−C3	1.384(4)
Ni−N4	2.123(3)	C3−C4	1.373(4)
H1−F1	1.42	C4−C5	1.391(3)
H1−F2	1.19	B1−F3	1.402(3)
F1−H1−F2	151	B1−F6	1.388(3)
F1−Ni−F2	178.00(6)	N1−Ni−N2	87.24(7)
F1−Ni−N1	88.87(7)	N1−Ni−N3	178.48(7)
F1−Ni−N3	90.07(7)	N1−Ni−N4	93.51(7)
F1−Ni−N4	91.21(7)	N2−Ni−N4	178.43(7)
F2−Ni−N4	90.69(7)	N3−Ni−N4	85.42(7)

Magnetization Studies. The temperature-dependence of the magnetization was measured using a Quantum Design MPMS 7 T SQUID magnetometer equipped with a standard sample transport. A polycrystalline sample was coated in high vacuum grease, loaded into a gelatin capsule, mounted in a plastic drinking straw, and affixed to the end of a stainless steel/brass rod. The sample rod was loaded into the instrument at 300 K, the magnetic field charged to 0.1 T, and data collected upon cooling down to a base temperature of 2 K. All

dx.doi.org/10.1021/ic300111k | Inorg. Chem. 2012, 51, 7520−7528

magnetic data were corrected for core diamagnetism using values typical of the constituent atoms and TIP of the Ni(II) ion.

The pulsed-field magnetization experiments (up to 60 T) used a 1.5 mm bore, 1.5 mm long, 1500-turn compensated-coil susceptometer, constructed from 50 gauge high-purity copper wire.[17] When a sample is within the coil, the signal voltage V is proportional to (dM/dt), where t is the time. Numerical integration of V is used to evaluate M. The sample is mounted within a 1.3 mm diameter ampule that can be moved in and out of the coil. Accurate values of M were obtained by subtracting empty coil data from that measured under identical conditions with the sample present. The susceptometer was placed inside a ^{3}He cryostat providing temperatures down to 0.5 K. The field H was measured by integrating the voltage induced in a ten-turn coil calibrated by observing the de Haas−van Alphen oscillations of the belly orbits of the copper coils of the susceptometer.

Heat Capacity. Data were obtained on polycrystalline samples of $[Ni(HF_2)(3\text{-Clpy})_4]BF_4$ using two apparati for different temperature regions. Between 2.5 and 100 K, the C_p was measured using a Quantum Design 14 T Physical Property Measurement System (PPMS). We mounted the sample (2.18 mg) on the platform using a small amount of Apiezon-N grease. During the mounting procedure, the Apiezon-N grease was melted by illumination with a filament lamp to ensure complete sample coverage so as to prevent solvent loss under high vacuum condition. Below 10 K, a homemade relaxation type calorimeter was applied to measure C_p. The small amount of polycrystalline sample (2.88 mg) was mixed with Apiezon-N grease and hand-pressed between single crystalline Si plates to obtain good temperature homogeneity. The calorimeter was mounted in an Oxford 15 T superconducting magnet system capable of reaching a base temperature of 0.4 K. Heat capacity data were obtained by traditional relaxation[18] and dual-slope methods.[19] For the latter method, the sample temperature was changed through a broad temperature range, and the $C_p(T)$ in this interval was evaluated from both of heating and cooling curves. The advantage of this technique made it possible to quickly measure C_p as a function of both temperature and magnetic field. The addenda C_p due to Apiezon-N, Si plates, and sample holder platform was measured separately. After subtracting the addenda contribution from the total specific heat, the sample C_p was obtained. Excellent agreement (within ∼5%) between the two techniques was achieved.

Muon-Spin Relaxation (μ^+SR). Zero-field (ZF) μ^+SR studies were made on a polycrystalline sample of $[Ni(HF_2)(3\text{-Clpy})_4]BF_4$ using the Low Temperature Facility (LTF) instrument at the Swiss Muon Source. For the measurement, the sample was mounted on a silver plate which was attached to the coldfinger of a dilution refrigerator.

In a μ^+SR experiment,[20] spin-polarized positive muons are stopped in a target sample, where the muon usually occupies an interstitial position in the crystal. The observed property in the experiment is the time evolution of the muon spin polarization, the behavior of which depends on the local magnetic field at the muon site. Each muon decays, with an average lifetime of 2.2 μs, into two neutrinos and a positron, the latter particle being preferentially emitted along the instantaneous direction of the muon spin. Recording the time dependence of the positron emission directions therefore allows the determination of the spin-polarization of the ensemble of muons. In our experiments, positrons are detected by detectors placed forward (F) and backward (B) of the initial muon polarization direction. Histograms $N_F(t)$ and $N_B(t)$ record the number of positrons detected in both detectors as a function of time following the muon implantation. The quantity of interest is the decay positron asymmetry function, defined as $A(t) = [N_F(t) - \alpha_{exp}N_B(t)]/[N_F(t) + \alpha_{exp}N_B(t)]$, where α_{exp} is an experimental calibration constant. $A(t)$ is proportional to the spin polarization of the muon ensemble.

Density-Functional Theory. For evaluation of the exchange couplings, the broken-symmetry (BS) approach of Noodleman[21] as implemented in the ORCA ver. 2.8 suite of programs[22,23] was employed. The formalism of Yamaguchi, which employs calculated expectation values $\langle S^2\rangle$ for both high-spin and broken-symmetry states was used.[24] The PBE0 functional was used in conjunction with the Ahlrichs-VTZ basis function set.[25] Spin densities were visualized using the UCSF Chimera program ver. 1.5.3.

Ligand-Field (LF) Modeling. Calculations were performed using the program package LIGFIELD.[26] All calculations employed the complete $3d^8$ electron configuration of the Ni(II) ion. Parameter fits were made by iterative rediagonalizations of the full matrices. The χ^2 minimizations were done by use of a Leuwenberg−Marquardt algorithm using equal weights for all observations. The quoted uncertainties on parameters are scaled values ensuring that the model will pass statistics. They are in most cases upper bounds on the actual uncertainties which would be obtained by a rigorous treatment including errors based on the observations.

RESULTS AND DISCUSSION

Crystal Structure. An ORTEP diagram along with atom labeling scheme is given in Figure 1a. It was found that the Ni(II) ion is surrounded by six ligands in a compressed NiN_4F_2 octahedral geometry. The four equatorial sites are occupied by N-donor atoms from 3-Clpy ligands at slightly different distances [Ni−N_{ave} = 2.124(2) Å] whereas the axial positions are taken by F-donors [Ni−F1 = 1.967(2) and Ni−F2 = 2.096(2) Å] as provided by the HF_2^- ligands. The relative distortion of the NiN_4F_2 octahedron, barring angular contributions, is 6.6% and exceeds that of $[Ni(HF_2)(pyz)_2]$-SbF_6 which is only 1.1%.[5] Chloro-substituents of *trans*-ligated 3-Clpy ligands lie on opposing sides of the NiN_4 plane because of a pseudo inversion center on the Ni(II) site.

The bifluoride H-atom was located on the electron density difference map and lies off of the F···F midpoint, creating an F1···H1···F2 bond angle of 151°. Strongly asymmetric H···F bonds were also found with the H1···F1 and H1···F2 distances being 1.42 and 1.19 Å, respectively. The distortion of the HF_2^- bridge is also manifested in its nonlinear coordination to the Ni(II) center, giving respective Ni−F1···H1 and Ni−F2···H1 bond angles of 153 and 131°. As compared to $[M(HF_2)(pyz)_2]X$ (M = Cu, Ni) and $Cu(HF_2)_2(pyz)$,[3−6] the HF_2^- molecular geometry is more unusual in $[Ni(HF_2)(3\text{-Clpy})_4]BF_4$ and reflects the flexibility and strength of such bonds.

$[Ni(HF_2)(3\text{-Clpy})_4]BF_4$ forms infinite 1D zigzag chains that propagate along the *c*-axis because of the bridging of adjacent NiN_4F_2 octahedra by HF_2^- ligands (Figure 1b). The chains feature uniform Ni···Ni separations of 6.237(5) Å, and as shown in Figure 1b, adjacent NiN_4F_2 octahedra are alternately tilted along the chain such that every other octahedron has the same configuration. Figure 1c shows that large interchain Ni···Ni separations of no less than 10.28 Å are ensured by the bulky 3-Clpy ligands and interstitial BF_4^- ions that pack in between them. Close Cl···Cl contacts of 3.687, 3.689, and 3.742 Å lie just beyond the sum of their van der Waals radii ($\sum r_{vdw}$ = 3.50 Å). As a result of these extremely weak interchain interactions, we predict the magnetism of $[Ni(HF_2)(3\text{-Clpy})_4]BF_4$ to be quasi-1D.

Electronic Spectroscopy and Ligand-Field (LF) Analysis. Solid state UV−vis absorption data (Figure 2) were recorded at 298 K and analyzed using the AOM.[27] The spectrum was approximated as a sum of a constant baseline and six independent Gaussian bands which gave good reproduction of the data.

The resulting transition energies (cm^{-1}) and associated assignments in octahedral (O) and tetragonal (D_4) symmetry are: 8750 [$^3T_2(O)E(D_4)$], 10530 [$^3T_2(O)B_2(D_4)$], 13270 [$^1E(O)A_1$, $B_1(D_4)$], 16100 ($^3T_1(O)E$, $A_2(D_4)$], 22100 ($^1T_2(O)E$, $B_2(D_4)$], and 26580 ($b^3T_1(O)E$, $A_2(D_4)$]. The assignments were made by combination of the AOM and

dx.doi.org/10.1021/ic300111k | Inorg. Chem. 2012, 51, 7520−7528

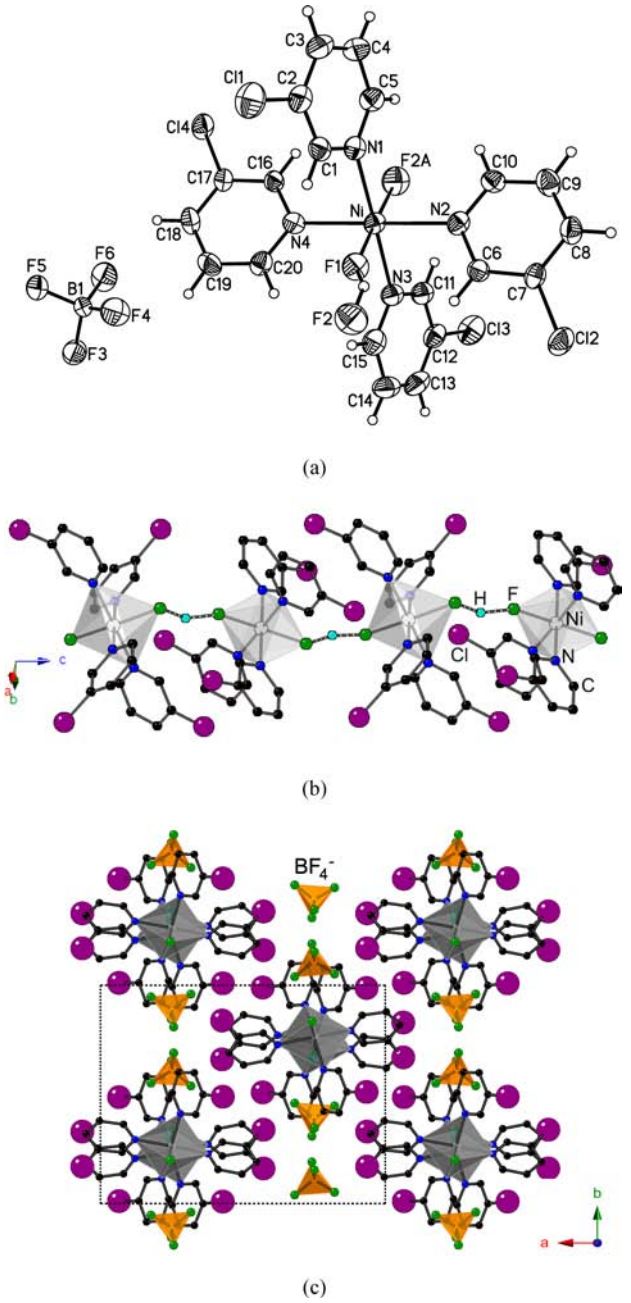

Figure 1. (a) ORTEP drawing and atom labeling scheme for $[Ni(HF_2)(3\text{-}Clpy)_4]BF_4$. Thermal ellipsoids are drawn at the 35% probability level. (b) Segment of a 1D chain. (c) Chain packing viewed parallel to the *c*-axis.

literature assignments for related Ni(II) complexes such as $[Ni(HF_2)(pyz)_2]X$.[5,6] Reasonable ligand-field (LF) parameters also allow the alternative assignment of the highest observed spin-forbidden transition (22100 cm^{-1}) to $^1A_1(O)$. However, in tetragonal symmetry, the transition to $^1A_1(D_4)$ is symmetry-forbidden, while transitions to both tetragonal components $^1T_2(O)B_2(D_4)$ and $^1T_2(O)E(D_4)$ are symmetry allowed, making this assignment the most plausible.

To avoid overparametrization of the AOM, the interelectronic repulsion was described using a single parameter with the ratio of Racah parameters fixed at $C/B = 4.25$.[28] Additionally, both bifluoride and 3-chloropyridine were assumed to be linearly ligating. For the latter ligands, this approximation is

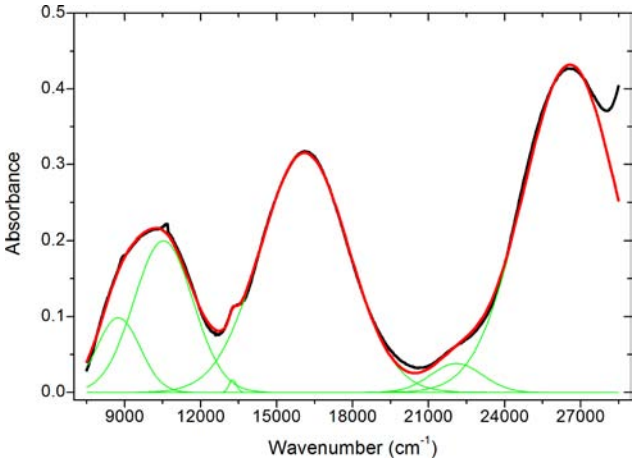

Figure 2. Gaussian deconvolution of the UV−vis absorption spectrum for $[Ni(HF_2)(3\text{-}Clpy)_4]BF_4$. Black: experimental data, green: individual Gaussians, red: sum of Gaussians.

justified by the twisting of the pyridine ring planes with respect to the direction of the main axial (tetragonal) component of the ligand field. With 45° twist angles, the approximation would be strictly correct.[29]

The six observed bands were accordingly parametrized using the following parameters; e_σ^{FHF}, e_π^{FHF}, e_σ^{Clpy}, e_π^{Clpy}, and *B*. This was performed for both an idealized tetragonal symmetry with orthoaxial ligators and for the experimentally determined coordination geometry. Results are summarized in Table 3. It

Table 3. AOM and Repulsion Parameter Values (cm^{-1}) Determined from Fitting of the 298 K Absorbance Spectrum

parameter	idealized D_4 symmetry	experimental geometry
e_σ^{FHF}	4312	3497
e_π^{FHF}	1343	660
e_σ^{Clpy}	3232	3613
e_π^{Clpy}	−220	0 (fixed)
B	848	836
rms dev.[a]	118	145
max. dev.[b]	201	592

[a]Root mean-square deviation in band positions. [b]Maximal absolute deviation in band position.

should be noted that the four LF parameters are quite heavily correlated for this set of observations, and assignment of individual confidence levels is meaningless. For the experimental geometry, this correlation necessitated fixation of one of the LF parameters. Since e_π^{Clpy} was determined to be of the same magnitude as the errors in the determined band positions, it was omitted.

Reproducibility of the band positions is fair, with absolute deviations below 200/600 cm^{-1} for the idealized/experimental geometries. Given the resolution of the data and since the deviations are less than or comparable to the spin−orbit coupling for Ni(II) ion, no better agreement can be expected. The values determined compare sensibly with literature data for related systems. In particular, it should be noted that the quite high values of e_σ^{FHF} and e_π^{FHF} as compared to the corresponding values for $[Ni(HF_2)(pyz)_2]ZF_6$ (Z = P, Sb) are anticipated because of the significantly shorter Ni−F bond lengths in the present system (1.967 Å vs 2.024/2.099 Å).[5] For an r^{-5} variation of the LF parameters, this translates into a 15−

dx.doi.org/10.1021/ic300111k | Inorg. Chem. 2012, 51, 7520−7528

38% increase in these. Both the σ- and π-parameter values for 3-chloropyridine are smaller than those previously reported for pyridine (e_σ^{py} = 4243 cm^{-1}, e_π^{py} = 438 cm^{-1}) in *trans*-$NiCl_2(py)_4$.[30] This is not unexpected because of the inductive effect of the Cl-substituent, but also the much higher donor strength of the bifluoride ligands as compared to Cl^- may invalidate the assumption of parameter transferability and contribute to the observed difference.

T-Dependent Magnetic Properties. Magnetic susceptibility data were obtained for a polycrystalline sample of $[Ni(HF_2)(3\text{-Clpy})_4]BF_4$ (Figure 3a) using a SQUID magnetometer. Upon cooling from 300 K, $\chi(T)$ decreases smoothly reaching a broad hump near 6 K and then continues to rise slowly as the temperature is lowered to 2 K. $\chi(T)T$ (not shown) remains approximately constant until ~50 K, after which it decreases much more rapidly down to the base temperature. This behavior is likely due to concomitant antiferromagnetic (AFM) coupling between S = 1 Ni(II) sites as well as ZFS of the $^3B_{1g}$ ground state. We also mention that no features suggestive of a transition to long-range magnetic order (LRO) were evidenced by these data.

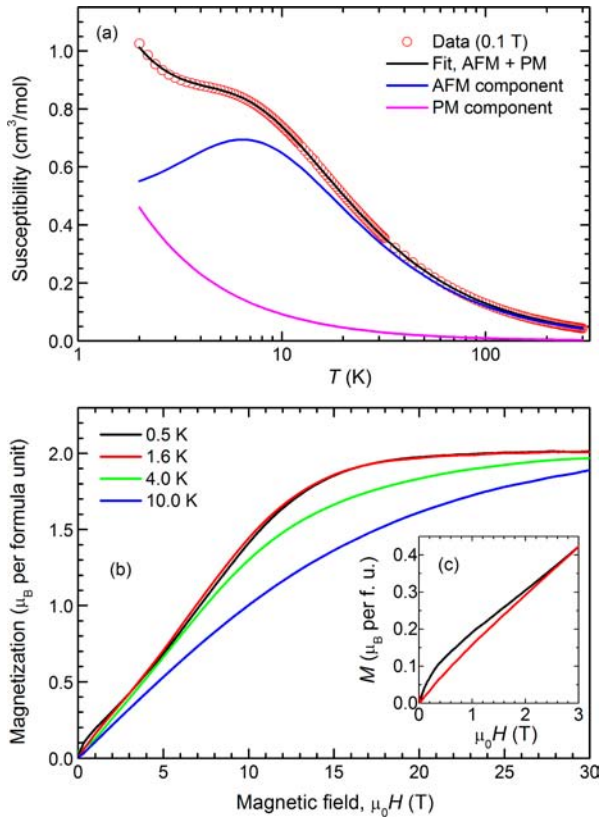

Figure 3. (a) χ vs T (O) obtained at 0.1 T. Black, blue, and purple lines denote the theoretical fit and the deconvoluted AFM and PM components, respectively, as described in the text. (b) Pulsed-field magnetization data for $[Ni(HF_2)(3\text{-Clpy})_4]BF_4$ acquired at several temperatures. (c) Low-T/-B region of $M(B)$ comparing 0.5 and 1.6 K data. The curvature in the 0.5 K data may originate from various sources as described in the text.

A preliminary assessment of the magnetic behavior of $[Ni(HF_2)(3\text{-Clpy})_4]BF_4$ came from a Curie–Weiss fit of the reciprocal magnetic susceptibility, $1/\chi(T) = 8(T - \theta)/Ng^2\mu_B^2S(S + 1)$, where S = 1. Fitting these data over the range 20 < T < 300 K led to g = 2.10(1) and θ = −7.5(1) K, the latter of which indicates possible AFM coupling between Ni(II) ions along the chain.

The nearly isolated magnetic chains in $[Ni(HF_2)(3\text{-Clpy})_4]BF_4$ render it possible to fit the $\chi(T)$ data to a S = 1 Heisenberg model. For the AFM spin Hamiltonian, $\hat{H} = J_{FHF}\sum S_i \cdot S_{i+1}$, that considers only the exchange interaction along the Ni-FHF-Ni pathway, we initially fitted $\chi(T)$ to the model developed by Weng[31] (for T > 8 K) to obtain the parameters, g = 2.08(1) and J_{FHF} = 4.60(3) K. Assuming that the low-T rise in $\chi(T)$ originates from noninteracting paramagnetic (PM) S = 1 spins (~7.1%), the fit can be extended over the entire T-range to give better quantitative agreement with final parameters; g = 2.10(1) and J_{FHF} = 4.86(3) K (black line in Figure 3a). Alternatively, the low-T tail in $\chi(T)$ may be intrinsic and possibly due to end-chain effects as shown to exist in $[Ni(C_3H_{10}N_2)_2(N_3)]ClO_4$ (NINAZ).[32] In either case, $\chi(T)$ will be similarly affected.

Inclusion of a mean-field correction term (zJ')[33] to account for residual interchain couplings did not alter the quality of the fit, thus suggesting good isolation of the 1D chains as expected. Despite the presence of single-ion anisotropy in this material (see below), such a model may still be expected to capture the effective low-energy behavior of the system. For cases where the anisotropy and exchange are comparable the exchange broadening of the anisotropy split levels should result in exchange-dominated behavior.

The broad maximum in $\chi(T)$, as determined from the blue curve labeled "AFM component" in Figure 3a, occurs at 6.5 K. This value of T_{max} can be used in the mean-field expression, $|J_{FHF}| = 2k_BT_{max}/2.70$,[34] to yield 4.81 K, which is in excellent agreement with the J_{FHF} obtained from the aforementioned fit of $\chi(T)$. This finding fully supports our quasi-1D description of the magnetism exhibited by $[Ni(HF_2)(3\text{-Clpy})_4]BF_4$.

Pulsed-Field Magnetization. Field-dependent magnetization (M) data (Figure 3b) were recorded using an extraction magnetometer and pulsed-magnetic fields of up to 60 T.[17] A sample could be cooled to temperatures as low as 0.50 K.[17] The T = 0.5 and 1.6 K curves essentially overlap and rise linearly from ~3 to 10 T. From Figure 3c however, an additional feature in the 0.5 K data may arise from paramagnetic impurities or end-chain effects. Thereafter the gradient of the $M(B)$ curve decreases until M saturates (becomes roughly constant) at around 20 T. The transition from linearly increasing to saturated behavior is broadened, as is often found for polycrystalline samples including $[Ni(HF_2)(pyz)_2]X$.[5,6] To locate the saturation field (B_c), linear extrapolations of the low and high-field data were made with their crossing point at 13.7(2) T being defined as B_c.[17] According to the above Hamiltonian, B_c and J_{FHF} are related by $g\mu_BB_c = 4J_{FHF}$, where μ_B is the Bohr magneton. Taking g = 2.10 (see above), a saturation field of B_c = 13.7(2) T suggests that J_{FHF} = 4.83(7) K, in good agreement with the values deduced from the susceptibility and mean-field prediction. The observed saturated moment of ~2 μ_B is expected for S = 1 with a g-factor close to 2.0.

Density-Functional Theory. To explore the strength of the exchange coupling across the bent bifluoride bridge, the 1D-chain was modeled by the dinuclear fragment *trans,trans*-$[(HF_2)Ni(3\text{-Clpy})_4(\mu\text{-FHF})Ni(3\text{-Clpy})_4(HF_2)]^+$, employing the experimental geometry determined from X-ray crystallography. The HDvV exchange coupling parameter J_{FHF} was calculated by the broken symmetry method and found to be 8.34 K (5.80 cm^{-1}). The exchange is calculated to be smaller than for systems with linear Ni-FHF-Ni bridging, *trans,trans*-$[(HF_2)Ni(pyz)_4(\mu\text{-FHF})Ni(pyz)_4(HF_2)]^+$, using the same

dx.doi.org/10.1021/ic300111k | Inorg. Chem. 2012, 51, 7520–7528

basis set and functional by a factor of about 1.7. It should be noted that the linear system actually features the longer Ni−Ni distance (6.343 Å vs 6.154 Å), but the shorter sum of bond lengths along the Ni-FHF-Ni bridge (6.343 Å vs 6.601 Å).[6]

A key revelation is that spin density does in fact reside on the proton of the HF_2^- bridge (Figure 4). Also of significance is

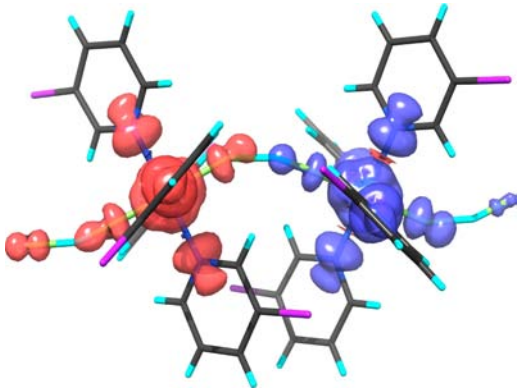

Figure 4. Calculated spin density for the singlet broken-symmetry state of *trans,trans*-$[(FHF)Ni(3\text{-}Clpy)_4(\mu\text{-}FHF)Ni(3\text{-}Clpy)_4(FHF)]^+$. Isosurface value is 0.0009. The "indented-octahedral" shape around the nickel centers closely resembles the one expected for a pure $(d_{x^2-y^2})^1(d_{z^2})^1$ electron configuration.

that H1 has the same spin polarization as the fluoride to which it is more closely associated (F2). If H1 had the opposite polarization, then we would have anticipated a FM spin polarization scheme such as Ni(↑)-F(↓)-H(↑)-F(↓)-Ni(↑), thus leading to FM coupling between Ni(II) ions which is inconsistent with the observed magnetic data. Instead, positive and negative spin density alternate along the Ni-FHF-Ni chains (i.e., is AFM) but relative to neighboring chains, the spin densities have the same sign (i.e., is FM). Since evidence for FM correlations in the $\chi(T)$ and $\chi(T)T$ data is absent, the interchain interaction must be very weak.

Zero-Field Splitting of the Ni(II) Ion. For a six-coordinate Ni(II) ion, a range of single-electron spin−orbit coupling constants ($375 < \zeta < 640$ cm^{-1}) can be used to compute the axial ZFS parameter (D) (Figure 5) based on the

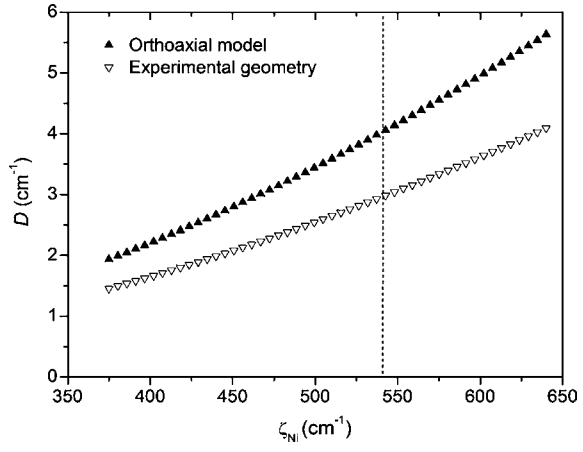

Figure 5. Axial zero-field splitting (D) calculated as a function of the one-electron spin−orbit coupling constant (ζ), using the AOM parameters. The dashed vertical line corresponds to a ζ-value reduced from the free-ion value by the same factor as the Racah B parameter.

aforementioned AOM analysis of the 300 K UV−vis absorption data.[27] This approach can yield an estimate of D since optical spectroscopy probes single-center transitions and is unaffected by the presence of exchange interactions which couple spins on different sites. The vertical line in Figure 5 denotes the ζ-value that is reduced from the free-ion value (668 cm^{-1}) by the same factor as the Racah B parameter, corresponding to $D \approx 3.0$ cm^{-1} (≈ 4.3 K) and $\zeta = 540$ cm^{-1} for the experimental geometry. As the radial dependences of the repulsion and spin−orbit parameters are not identical, they do not scale perfectly and so our value of ζ could be slightly overestimated. We estimate that the errors on ζ and D are about 20%. A positive D-value is suggestive of easy-plane (XY) anisotropy which is analogous to tetragonal $[Ni(HF_2)(pyz)_2]ZF_6$ (Z = P, Sb).[5,6] Both AOM and DFT agree that the $d_{x^2-y^2}$ magnetic orbital is higher in energy than the d_{z^2} orbital.

Search for LRO by μ^+SR and Heat Capacity. A representative zero-field μ^+SR spectrum measured at 0.5 K is shown in Figure 6. Across the entire measured temperature

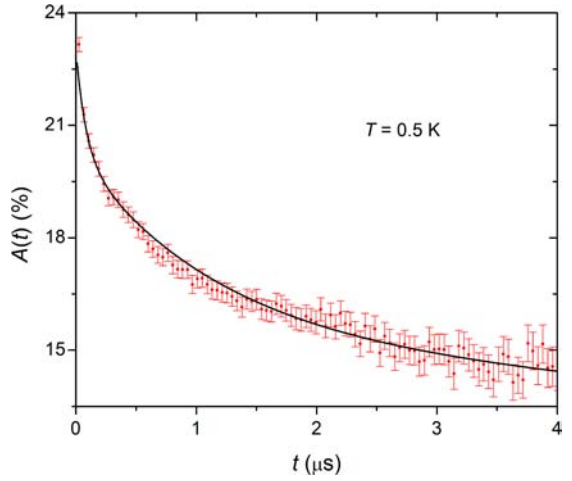

Figure 6. Zero-field μ^+SR data measured at 0.5 K. Exponential relaxation is observed across the entire measured temperature range, indicative of dynamic fluctuations of the local magnetic field distribution.

regime ($0.025 \leq T \leq 4.2$ K) the spectra relax monotonically. We do not observe any oscillations or shift in the baseline that might be expected for a transition to LRO. Instead, the spectra are well described by a relaxation function of the form, $A(t) = A_1e^{-\Lambda t} + A_2e^{-\lambda t} + A_{bg}$, where A_{bg} is the background contribution from those muons that stop in the sample holder or cryostat tail and the ratio A_1/A_2 was found to be approximately 0.5. The component with amplitude A_1 has a large relaxation rate $\Lambda \approx 12$ MHz. Such a component, which does not vary much with temperature, is often observed in the μ^+SR spectra of materials of this type. The smaller relaxation rate $\lambda = 0.9$ MHz was also found to be independent of temperature across the entire measured T-range.

We find no μ^+SR evidence for LRO in this material down to 0.025 K. The observed exponential relaxation is often indicative of dynamic fluctuations of the local magnetic field at the muon site[35] in the fast fluctuation regime. We note that a similar behavior was found in $Cu(HF_2)_2(pyz)$.[3]

Figure 7a displays the zero-field heat capacity (C_p) of $[Ni(HF_2)(3\text{-}Clpy)_4]BF_4$ where the absence of a λ-anomaly over the measured T-range preclude LRO in this material which is

dx.doi.org/10.1021/ic300111k | Inorg. Chem. 2012, 51, 7520−7528

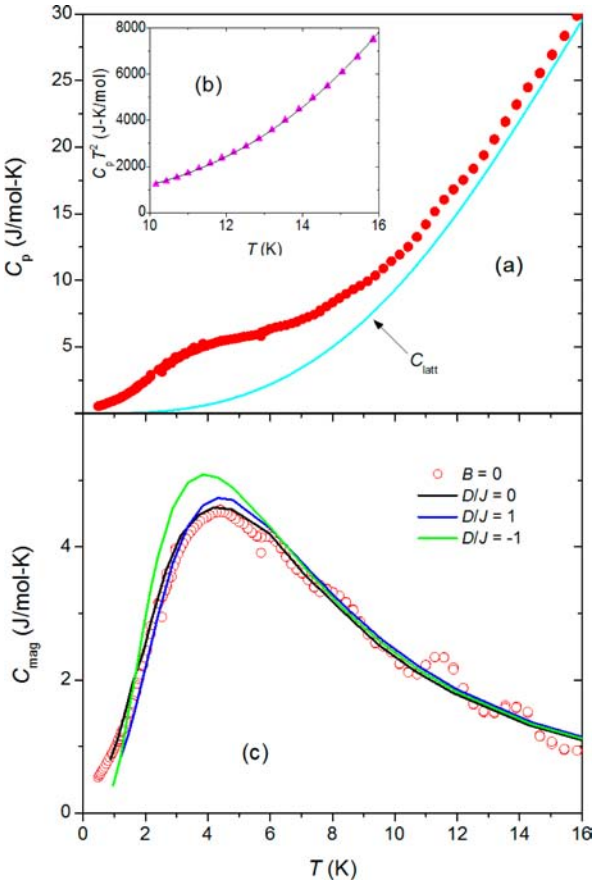

Figure 7. (a) Total heat capacity (red filled circles) measured at 0 T along with the estimated lattice contribution C_{latt} (cyan lines). (b) C_pT^2 vs T (magenta triangles) and fit (black lines) to $C_pT^2 = a + bT^5 + cT^7$. (c) Magnetic heat capacity C_{mag} (red open circles). Colored lines represent calculated C_{mag} curves for various D/J ratios as described in the text.

consistent with our μ^+SR findings. Instead, a broad peak was observed, the origin of which is attributed to low-dimensional spin correlations and/or a Schottky anomaly associated with the ZFS of the Ni(II) ion. It is well-known that the total heat capacity (C_p) is the sum of magnetic (C_{mag}) and lattice contributions (C_{latt}). The magnetic contribution can be approximated by a/T^2 in a high-temperature series expansion whereas C_{latt} can be estimated by $bT^3 + cT^5$. By plotting C_pT^2 vs T (Figure 7b), we found a sublinear dependence of the data over a certain interval.[36] A fit of those data gave a = 267(15) J·K/mol, b = 0.0106(2) J·K^4/mol, and $c = -1.33(4) \times 10^{-5}$ J·K^6/mol. Applying De Klerk's formula derived for a Heisenberg magnet, the relation $a = 2RzJ_{FHF}^2/3k_B^2$ is obtained for S = 1.[37] We obtain J_{FHF} = 4.9(2) K (for z = 2) which nicely agrees with the value found from the $\chi(T)$ fit.

Subtracting C_{latt} from C_p leads to C_{mag} which shows a broad peak centered at 4.3 K (Figure 7c). Because the spin exchange and ZFS both may be important in $[Ni(HF_2)(3\text{-}Clpy)_4]BF_4$, we compare C_{mag} to theoretical curves derived by Blöte for the S = 1 Heisenberg chain model that simultaneously considers various ratios of the anisotropy D/J.[38] We should point out that the simulated curves are scaled only against our susceptibility-derived J_{FHF} value. The experimental and theoretical curves are largely indiscriminant for $T \geq 6$ K; however, clear deviations occur below this temperature. Statistically, D/J = 0 and 1 are not grossly different (over the whole T-range) whereas $D/J = -1$ does not describe the data nearly as well. These findings suggest that the D/J ratio lies between 0 and 1 as expected based on the experimental data in hand. We can rule out a Haldane system as the predicted low-T exponential behavior of C_{mag} was not observed.[9,39]

Figure 8 shows the temperature dependence of C_{mag}/T at several magnetic fields. From this plot, the zero-field anomaly is

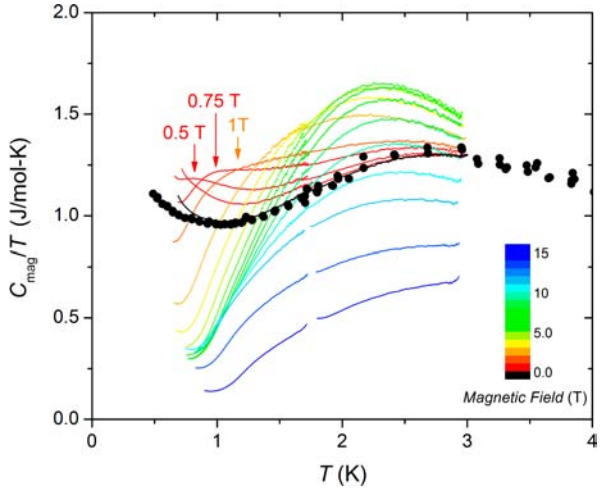

Figure 8. C_{mag}/T vs T under various magnetic fields. The curves were obtained using the dual slope method whereas the points were measured using the traditional relaxation method.

located at 2.8 K. The application of a magnetic field moves the broad peak to lower temperature while increasing its peak height up to 4 T. Above 4 T, the anomaly becomes even broader and its amplitude decreases. When the applied field strength is less than 1 T, we can find an additional field-induced anomaly (indicated by arrows). This anomaly is broad and cannot be attributed to LRO of spins. The peak temperature of the field-induced anomaly monotonically grows as the field increased. Above 2 T, the field-induced and zero-field anomalies merge and are no longer recognized as independent features.

Figure 9 shows the same C_{mag}/T data in the form of a contour plot. As shown by the black dashed line, the field-induced peak rapidly shifts to higher temperatures as the field increased. The behavior is sometimes manifested as a Zeeman splitting of the magnetic level, which induces a field-dependent Schottky anomaly.[40] However, if we consider Zeeman splitting of free spins for example, the C_{mag}/T peak of the Schottky anomaly is expected to occur at higher fields as indicated by the red (S = 1/2)[40,41] and blue (S = 1)[41] dashed lines which is inconsistent with the rapid change in observed behavior.

Since application of a magnetic field can modify the ground state of a 1D system,[41−44] it is tempting to speculate that the field-induced hump might be related to the crossover from paramagnetic to an exotic low-dimensional ground state, such as XY-AFM,[45] gapless chiral,[46] or gapless Luttinger-Liquid (LL).[47] A quasi-1D bond-alternating chain system, $[Ni(C_9H_{24}N_4)_2(NO_2)]$-$ClO_4$ (NTENP), reportedly exhibits broad humps in the field-dependent heat capacity which was attributed to a LL-like behavior.[48] We find strikingly similar behavior in $[Ni(HF_2)(3\text{-}Clpy)_4]BF_4$, where in spite of a uniform chain motif, the NiN_4F_2 octahedra alternately tilt along the chain. So far the LL phase has mainly been studied in S = 1/2 Cu(II) systems, for example $(Hpip)_2CuBr_4$.[42] A gapless

dx.doi.org/10.1021/ic300111k | Inorg. Chem. 2012, 51, 7520−7528

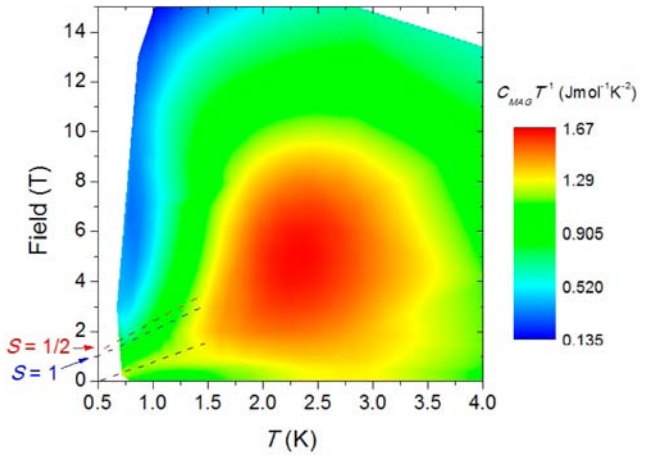

Figure 9. Contour plot of C_{mag}/T. The black dashed line is a guide to the eye to identify the shift in the small peak. The red and blue dashed lines denote the calculated temperature and magnetic field dependence of a Schottky anomaly (if it existed). See Supporting Information, Figure S1.

chiral ordered phase might account for the field-induced ground state in $[Ni(HF_2)(3\text{-Clpy})_4]BF_4$. This phase is expected in the 1D zigzag $S = 1$ spin system with XY spin anisotropy. This behavior may contribute to the low-T upturn in $\chi(T)$ that we initially ascribed to uncorrelated spins.

CONCLUSIONS

The crystal structure of $[Ni(HF_2)(3\text{-Clpy})_4]BF_4$ consists of 1D zigzag chains whereby NiN_4F_2 octahedra are linked only by HF_2^- ligands. Interestingly, the HF_2^- ligand is strongly distorted with H···F bond lengths of 1.19 and 1.42 Å and an F···H···F bond angle of 151°. Surprisingly, the asymmetry does not greatly hinder efficient spin exchange along the Ni-FHF-Ni chains, and DFT calculations confirm that all three atoms of the HF_2^- bridge bear significant spin density. Fitting the $\chi(T)$ data to a 1D Heisenberg chain model yielded $|J_{FHF}| = 4.86$ K, a value fully consistent with those derived from pulsed-field magnetization and heat capacity data. AOM parametrization of UV−vis spectral data provided several ligand-field parameters including the zero-field splitting (D) ≈ 3.0 cm^{-1} (≈ 4.3 K), which is smaller than those of $[Ni(HF_2)(pyz)_2]ZF_6$ (Z = P, Sb). The values of D and $|J_{FHF}|$ obtained in this way are comparable in magnitude leading to the conclusion that the D/J ratio is expected to be appreciably different from zero and possibly of order unity. Such a D/J ratio, as well as the complete absence of any evidence for a spin gap, precludes existence of the Haldane phase. The apparently negligible interchain interactions further prevent XY magnetic order, at least down to 0.025 K. The broad low temperature peak in $C_{mag}(T)$ cannot be attributed to a Schottky anomaly but instead likely arises from 1D spin correlations in this material. Further experiments on single crystals are planned to better understand the exotic field-induced phase, and work is continuing along these lines.

ASSOCIATED CONTENT

Supporting Information

CIF for $[Ni(HF_2)(3\text{-Clpy})_4]BF_4$ and calculated (B, T)-dependence of the $S = 1/2$ and $S = 1$ Schottky anomaly. This material is available free of charge via the Internet at http://pubs.acs.org.

AUTHOR INFORMATION

Corresponding Author

*E-mail: jmanson@ewu.edu.

Present Address

[V]Department of Physics, Durham University, Durham, DH1 3LE, U.K.

Notes

The authors declare no competing financial interest.

ACKNOWLEDGMENTS

The work at EWU was supported by the National Science Foundation (NSF) under Grant DMR-1005825. Research performed at North Carolina State University was supported by the Office of Basic Energy Sciences (BES), Division of Materials Sciences of the U.S. Department of Energy (DoE) under Grant DE-FG02-86ER45259 and by the computing resources of the NERSC and HPC Centers. A portion of this work was performed at the National High Magnetic Field Laboratory, which is supported by NSF Cooperative Agreement No. DMR-0654118, the State of Florida, and the U.S. DoE BES program "Science in 100 T." Support of the EPSRC, U.K., is gratefully acknowledged, and some of this work made use of the Swiss Muon Source, Paul Scherrer Institut, CH.

REFERENCES

(1) (a) Emsley, J.; Parker, R. J.; Overill, R. E. *J. Chem. Soc., Faraday Trans. 2* **1982**, *79*, 1347. (b) Pendas, A. M.; Blanco, M. A.; Francisco, E. *J. Chem. Phys.* **2006**, *125*, 184112. (c) Clark, J. H.; Emsley, J.; Jones, D. J.; Overill, R. E. *J. Chem. Soc., Dalton Trans.* **1981**, 1219. (d) Fujiwara, F. Y.; Martin, J. S. *J. Am. Chem. Soc.* **1974**, *96*, 7625. (e) Keil, F.; Ahlrichs, R. *J. Am. Chem. Soc.* **1976**, *98*, 4787.

(2) Larson, J. W.; McMahon, T. B. *J. Am. Chem. Soc.* **1982**, *104*, 5848.

(3) Manson, J. L.; Warter, M. L.; Schlueter, J. A.; Lancaster, T.; Steele, A. J.; Blundell, S. J.; Pratt, F. L.; Singleton, J.; McDonald, R. D.; Lee, C.; Whangbo, M.-H.; Plonczak, A. *Angew. Chem., Int. Ed.* **2011**, *50*, 1573.

(4) (a) Manson, J. L.; Schlueter, J. A.; Funk, K. A.; Southerland, H. I.; Twamley, B.; Lancaster, T.; Blundell, S. J.; Baker, P. J.; Pratt, F. L.; Singleton, J.; McDonald, R. D.; Goddard, P. A.; Sengupta, P.; Batista, C. D.; Ding, L.; Lee, C.; Whangbo, M.-H.; Franke, I.; Cox, S.; Baines, C.; Trial, D. *J. Am. Chem. Soc.* **2009**, *131*, 6733. (b) Manson, J. L.; Conner, M. M.; Schlueter, J. A.; Lancaster, T.; Blundell, S. J.; Brooks, M. L.; Pratt, F. L.; Papageorgiou, T.; Bianchi, A. D.; Wosnitza, J.; Whangbo, M.-H. *Chem. Commun.* **2006**, 4894. (c) Cizmar, E.; Zvyagin, S. A.; Beyer, R.; Uhlarz, M.; Ozerov, M.; Skourski, Y.; Manson, J. L.; Schlueter, J. A.; Wosnitza, J. *Phys. Rev. B* **2010**, *81*, 064422. (d) Brown, S.; Cao, J.; Musfeldt, J. L.; Conner, M. M.; McConnell, A. C.; Southerland, H. I.; Manson, J. L.; Schlueter, J. A.; Phillips, M. D.; Turnbull, M. M.; Landee, C. P. *Inorg. Chem.* **2007**, *46*, 8577. (e) Musfeldt, J. L.; Vergara, L. I.; Brinzari, T. V.; Lee, C.; Tung, L. C.; Kang, J.; Wang, Y. J.; Schlueter, J. A.; Manson, J. L.; Whangbo, M.-H. *Phys. Rev. Lett.* **2009**, *103*, 157401. (f) Sengupta, P.; Batista, C. D.; McDonald, R. D.; Cox, S.; Singleton, J.; Huang, L.; Papageorgiou, T. P.; Ignatchik, O.; Herrmannsdorfer, T.; Manson, J. L.; Schlueter, J. A.; Funk, K. A.; Wosnitza, J. *Phys. Rev. B* **2009**, *79*, 060409(R). (g) Manson, J. L.; Schlueter, J. A.; McDonald, R. D.; Singleton, J. *J. Low Temp. Phys.* **2010**, *159*, 15.

(5) Manson, J. L.; Lapidus, S. H.; Stephens, P. W.; Peterson, P. K.; Carreiro, K. E.; Southerland, H. I.; Lancaster, T.; Blundell, S. J.; Steele, A. J.; Goddard, P. A.; Pratt, F. L.; Singleton, J.; Kohama, Y.; McDonald, R. D.; Del Sesto, R. E.; Smith, N. A.; Bendix, J.; Zvyagin, S. A.; Kang, J.; Lee, C.; Whangbo, M.-H.; Zapf, V. S.; Plonczak, A. *Inorg. Chem.* **2011**, *50*, 5990.

(6) Manson, J. L.; Carreiro, K. E.; Lapidus, S. H.; Stephens, P. W.; Goddard, P. A.; Del Sesto, R. E.; Bendix, J.; Franke, I.; Ghannadzedah,

S.; Singleton, J.; Lancaster, T.; Möller, J. S.; Baker, P. J.; Pratt, F. L.; Blundell, S. J.; Kang, J.; Lee, C.; Whangbo, M.-H. *Dalton Trans.* **2012**, *41*, 7235.
(7) (a) Halder, G. J.; Chapman, K. W.; Schlueter, J. A.; Manson, J. L. *Angew. Chem., Int. Ed.* **2011**, *50*, 419. (b) Manson, J. L.; Conner, M. M.; Schlueter, J. A.; McConnell, A. C.; Southerland, H. I.; Malfant, I.; Lancaster, T.; Blundell, S. J.; Brooks, M. L.; Pratt, F. L.; Singleton, J.; McDonald, R. D.; Lee, C.; Whangbo, M.-H. *Chem. Mater.* **2008**, *20*, 7408. (c) Musfeldt, J. L.; Liu, Z.; Li, S.; Kang, J.; Lee, C.; Jena, P.; Manson, J. L.; Schlueter, J. A.; Carr, G. L.; Whangbo, M.-H. *Inorg. Chem.* **2011**, *50*, 6347. (d) Goddard, P. A.; Singleton, J.; Maitland, C.; Blundell, S. J.; Lancaster, T.; Baker, P. J.; McDonald, R. D.; Cox, S.; Sengupta, P.; Manson, J. L.; Funk, K. A.; Schlueter, J. A. *Phys. Rev. B* **2008**, *78*, 052408. (e) Schlueter, J. A.; Park, H.; Manson, J. L.; Nakotte, H.; Schultz, A. J. *Phys. B* **2010**, *405*, S324. (f) Conner, M.; McConnell, A.; Schlueter, J.; Manson, J. *J. Low Temp. Phys.* **2006**, *142*, 273.
(8) Haldane, F. D. M. *Phys. Rev. Lett.* **1983**, *50*, 1153.
(9) Affleck, I. *J. Phys.: Condens. Matter* **1989**, *1*, 3047.
(10) Sakai, T.; Takahashi, M. *Phys. Rev. B* **1990**, *42*, 4537.
(11) Wierschem, K.; Sengupta, P. arXiv:1108.1648.
(12) Takeuchi, T.; Ono, M.; Hori, H.; Yosida, T.; Yamagishi, A.; Date, M. *J. Phys. Soc. Jpn.* **1992**, *61*, 3255.
(13) *APEX II*, 1.08; Bruker AXS, Inc.: Madison, WI, 2004.
(14) *SAINT+*, 7.06; Bruker AXS, Inc.: Madison, WI, 2003.
(15) *SADABS*, 2.03; Sheldrick, G. University of Göttingen: Göttingen, Germany, 2001.
(16) *SHELXTL*, 6.14; Bruker AXS, Inc.: Madison, WI, 2000.
(17) Goddard, P. A.; Singleton, J.; Sengupta, P.; McDonald, R. D.; Lancaster, T.; Blundell, S. J.; Pratt, F. L.; Cox, S.; Harrison, N.; Manson, J. L.; Southerland, H. I.; Schlueter, J. A. *New J. Phys.* **2008**, *10*, 083025.
(18) Bachmann, R.; DiSalvo, F. J.; Geballe, T. H.; Greene, R. L.; Howard, R. E.; King, C. N.; Kirsch, H. C.; Lee, K. N.; Schwall, R. E.; Thomas, H.-U.; Zubeck, R. B. *Rev. Sci. Instrum.* **1972**, *43*, 205.
(19) Riegel, S.; Weber, G. *J. Phys. E: Sci. Instrum.* **1986**, *19*, 790.
(20) Blundell, S. J. *Contemp. Phys.* **1999**, *40*, 175.
(21) Noodleman, L. *J. Chem. Phys.* **1981**, *74*, 5737.
(22) Neese, F. *ORCA*, Version 2.8, revision 2131; Institut für Physikalische und Theoretische Chemie, Universitaet Bonn: Bonn, Germany, 2010.
(23) (a) Neese, F. *Coord. Chem. Rev.* **2009**, *253*, 526. (b) Sinnecker, S.; Neese, F.; Lubitz, W. *J. Biol. Inorg. Chem.* **2005**, *10*, 231.
(24) (a) Yamaguchi, K.; Takahara, Y.; Fueno, T. In *Applied Quantum Chemistry*; Smith, V. H., Schafer, F., III, Morokuma, K., Eds.; D. Reidel: Boston, MA, 1986; p 155. (b) Soda, T.; Kitagawa, Y.; Onishi, T.; Takano, Y.; Shigeta, Y.; Nagao, H.; Yoshioka, Y.; Yamaguchi, K. *Chem. Phys. Lett.* **2000**, *319*, 223.
(25) Schaefer, A.; Horn, H.; Ahlrichs, R. *J. Chem. Phys.* **1992**, *97*, 2571.
(26) Bendix, J. *Compr. Coord. Chem. II* **2004**, *2*, 673.
(27) Schäffer, C. E.; Jørgensen, C. K. *Mol. Phys.* **1965**, *9*, 401.
(28) Bendix, J.; Brorson, M.; Schaffer, C. E. *Inorg. Chem.* **1993**, *32*, 2838.
(29) Schäffer, C. E. *Struct. Bond. (Berlin)* **1968**, *5*, 68.
(30) Kurzak, K.; Kolkowicz, A. *Spectrochim. Acta* **1990**, *46A*, 1231.
(31) (a) Weng, C. Y. Ph.D. Thesis, Carnegie-Mellon University, Pittsburgh, PA, 1968. (b) Meyer, A.; Gleizes, A.; Gerard, J. J.; Verdaguer, M.; Kahn, O. *Inorg. Chem.* **1982**, *21*, 1729.
(32) Granroth, G. E.; Maegawa, S.; Meisel, M. W.; Krzystek, J.; Brunel, L.-C.; Bell, N. S.; Adair, J. H.; Ward, B. H.; Fanucci, G. E.; Chou, L.-K.; Talham, D. R. *Phys. Rev. B* **1998**, *58*, 9312.
(33) Ginsberg, A. P.; Lines, M. E. *Inorg. Chem.* **1972**, *11*, 2289.
(34) Miedema, A. R.; de Jongh, L. J. *Adv. Phys.* **1974**, *23*, 1.
(35) Hayano, R. S.; Uemura, Y. J.; Imazato, J.; Nishida, N.; Yamazaki, T.; Kubo, R. *Phys. Rev. B* **1979**, *20*, 850.
(36) For example, see Orendáčová, A.; Zorkovská, A.; Park, J.-H.; Orendáč, M.; Trávniček, Z.; Feher, A.; Meisel, M. W. *Phys. Status Solidi C* **2006**, *3*, 134.
(37) De Klerk, D. *Phys. B* **1946**, *12*, 513.
(38) Blöte, H. W. J. *Phys. B* **1975**, *79*, 427.
(39) Honda, Z.; Katsumata, K.; Nishiyama, Y.; Harada, I. *Phys. Rev. B* **2001**, *63*, 064420.
(40) Kohama, Y.; Tojo, T.; Kawaji, H.; Atake, T.; Matsuishi, S.; Hosono, H. *Chem. Phys. Lett.* **2006**, *421*, 558.
(41) See Figure S1 in the Supporting Information.
(42) Hagiwara, M.; Tsujii, H.; Rotundu, C. R.; Andrka, B.; Takano, Y.; Tateiwa, N.; Kobayashi, T. C.; Suzuki, T.; Suga, S. *Phys. Rev. Lett.* **2006**, *96*, 147203.
(43) Rüegg, C.; Kiefer, K.; Thielemann, B.; McMorrow, D. F.; Zapf, V.; Normand, B.; Zvonarev, M. B.; Bouillot, P.; Kollath, C.; Giamarchi, T.; Capponi, S.; Poilblanc, D.; Biner, D.; Krämer, K. W. *Phys. Rev. Lett.* **2008**, *101*, 247202 ; Hpip = piperidinium cation.
(44) Honda, Z.; Katsumata, K.; Nishiyama, Y.; Harada, I. *Phys. Rev. B* **2001**, *63*, 064420.
(45) Zong, X.; Suh, B. J.; Niazi, A.; Yan, J. Q.; Schlagel, D. L.; Lograsso, T. A.; Johnston, D. C. *Phys. Rev. B* **2008**, *77*, 014412.
(46) Miyazaki, H.; Hiwasa, T.; Harada, I. *J. Phys. (Paris)* **2006**, *51*, 167−170.
(47) Cuccoli, A.; Roscilde, T.; Vaia, R.; Verrucchi, P. *Phys. Rev. B* **2003**, *68*, 060402(R).
(48) Hikihara, T.; Kaburagi, M.; Kawamura, H.; Tonegawa, T. *J. Phys. Soc. Jpn.* **2000**, *69*, 259−266.